



Contents lists available at ScienceDirect

## Synthetic Metals

journal homepage: [www.elsevier.com/locate/synmet](http://www.elsevier.com/locate/synmet)Kinetics of interface state-limited hole injection in  $\alpha$ -naphthylphenylbiphenyl diamine ( $\alpha$ -NPD) thin layersGermà Garcia-Belmonte<sup>a,\*</sup>, Juan Bisquert<sup>a</sup>, Paulo R. Bueno<sup>b</sup>, C.F.O. Graeff<sup>c</sup>, F.A. Castro<sup>d</sup><sup>a</sup> Grup de Dispositius Fotovoltàics i Optoelectrònics, Departament de Física, Universitat Jaume I, ES-12071 Castelló, Spain<sup>b</sup> Universidade Estadual Paulista, Instituto de Química, C. Postal 355, CEP 14800-900, Araraquara, SP, Brazil<sup>c</sup> Departamento de Física, FC, Universidade Estadual Paulista, 17033-360 Bauru, Brazil<sup>d</sup> Empa, Swiss Federal Laboratories for Materials Testing and Research, Laboratory for Functional Polymers, Überland str. 129, CH-8600 Dübendorf, Switzerland

## ARTICLE INFO

## Article history:

Received 5 August 2008

Received in revised form 6 October 2008

Accepted 10 November 2008

Available online xxx

## PACS:

73.40.-c, 73.61.Ph, 73.43.Cd

## Keywords:

Organic light-emitting diodes

Injection-limited current

Metal-organic interfaces

Capacitance

## ABSTRACT

Injection-limited operation is identified in thin-film,  $\alpha$ -NPD-based diodes. A detailed model for the impedance of the injection process is provided which considers the kinetics of filling/releasing of interface states as the key factor behind the injection mechanism. The injection model is able to simultaneously account for the steady-state, current-voltage ( $J$ - $V$ ) characteristics and impedance response, and is based on the sequential injection of holes mediated by energetically distributed surface states at the metal-organic interface. The model takes into account the vacuum level offset caused by the interface dipole, along with the partial shift of the interface level distribution with bias voltage. This approach connects the low-frequency ( $\sim 1$  Hz) capacitance spectra, which exhibits a transition between positive to negative values, to the change in the occupancy of interface states with voltage. Simulations based on the model allow to derive the density of interface states effectively intervening in the carrier injection ( $\sim 5 \times 10^{12} \text{ cm}^{-2}$ ), which exhibit a Gaussian-like distribution. A kinetically determined hole barrier is calculated at levels located  $\sim 0.4$  eV below the contact work function.

© 2008 Elsevier B.V. All rights reserved.

## 1. Introduction

One of the most widely used hole-transporting materials (HTMs) in small molecule-based organic light-emitting devices (OLEDs) is the archetypical  $N,N'$ -diphenyl- $N,N'$ -bis(1-naphthylphenyl)-1,1'-biphenyl-4,4'-diamine ( $\alpha$ -NPD) [1,2]. Thin films made up of such molecules form hole-injection layers between the device anode, and the electron-transporting and luminescent compound.  $\alpha$ -NPD has been largely investigated to build green-emission OLEDs in combination with tris(8-hydroxyquinoline) aluminium ( $\text{Alq}_3$ ), and alternatively to act as host material in which a luminescent dopant is embedded [3]. As HTM, the key parameter to be determined is the mobility exhibited by holes. Hole-mobility values reported in the literature lie within the order of  $10^{-4} \text{ cm}^2 \text{ V}^{-1} \text{ s}^{-1}$ , either determined from time-of-flight transients [4,5] or admittance spectroscopy [6]. It is also well-known that holes make up the dominant carrier in  $\alpha$ -NPD as their mobility is higher by several orders of magnitude than that encountered for electrons. Moreover, it is assumed that the transport of holes in  $\alpha$ -NPD layers is governed by space-charge limited conduction (SCLC) [6], similarly to that occurring

in undoped (insulating) materials. This conduction model gives rise to  $J$ - $V$  characteristics which exhibit the behavior  $J \propto V^m$  with  $m \geq 2$ . The limiting case  $m=2$  is expected for trap-free transport mechanisms, while the case  $m > 2$  is usually interpreted in terms of trap-charge limited conduction with the parameter  $m-1 = E_t/k_B T$  being related to the characteristic energy of the exponential trap tail  $E_t$  [7,8]. The analysis of  $J$ - $V$  characteristics also may include the dependence of the mobility on temperature and electrical field  $F$  as  $\mu = \mu_0 \exp(\beta\sqrt{F})$  [9,10], and charge carrier density [11].

In any case a good approximation of the current level expected in a practical device, which is usually constructed by means of thin ( $L=50$ – $200$  nm) HTM layers, can be estimated by using the well-known expression valid for trap-free SCLC [12]

$$J_{\text{SCLC}} = \frac{9}{8} \varepsilon \varepsilon_0 \mu \frac{V^2}{L^3} \quad (1)$$

Here  $V$  corresponds to the operating voltage, and  $\varepsilon \approx 2-3$  represents the dielectric constant of the organic material ( $\varepsilon_0$  is the permittivity of the free space). A rough comparison between the current level calculated by means of Eq. (1) and the experimental  $J$ - $V$  characteristics might be employed to assess the extent in the Ohmic character of the contacts. An operational figure of merit for the supply efficiency of the contact is then given by the ratio  $J/J_{\text{SCLC}}$  [13]. In this sense, a contact is considered to be Ohmic if it is able

\* Corresponding author. Tel.: +34 964 728040.  
E-mail address: [garciag@uji.es](mailto:garciag@uji.es) (G. Garcia-Belmonte).

to inject enough current so as to fulfill the current demand of the organic bulk,  $J/J_{\text{SCLC}} = 1$ . In case of  $J/J_{\text{SCLC}} < 1$  the device operation is considered to be injection-limited. Following this procedure the partial Ohmic character of the indium tin oxide (ITO)/ $\alpha$ -NPD contact was evidenced by direct measurement of the hole mobility and comparison with the experimental  $J$ - $V$  curves [5]. Hole injection barriers at metal- $\alpha$ -NPD interfaces are generally larger than  $\sim 1$  eV even when high work function electrodes like Au and ITO are used, leading to devices which operate under injection-limitation [14,15].

The formation of surface dipole layers at the metal/organic or organic/organic interfaces is a well-established fact [16]. Interface dipole offsets the vacuum levels of the metal and the organic semiconductor, and it is able to produce a lowering of the energy levels in the first organic layers as large as 1 eV. The interface dipole may be either positive (electron injection improved) or negative (hole injection improved). Electronic states of organic layers neighboring the metallic contact are accessible by using ultraviolet (UPS) and inverse (IPS) photoelectron spectroscopies [16–19]. Another, related, effect is the formation of new metal-organic states by chemical bonding of the organic molecules at the interface [20], surface oxidation [21] or contamination [22].

Charge-carrier injection at metal-organic interfaces has been analyzed in terms of the diffusion-limited thermionic emission [23]. This approach has been improved by considering the injection into an energetically disordered organic solid as a sequential process in which carriers hop from the metal Fermi level to localized states, exhibiting Gaussian energy disorder, close to the interface [24,25]. Instead of considering the first hop from the metal Fermi level into the organic film as the energetically costly event, injection models have been developed which consider the determining role of intermediate states induced by interface dipoles [26,27]. More recent alternative approaches highlight the role of the filling/releasing kinetics of energetically distributed interface states [28,29]. It is then a crucial issue to reveal which preparing conditions or device structure determine particular current-limiting mechanisms.

The sole analysis of steady-state  $J$ - $V$  characteristics appears to be non-definitive in most cases. Proper model selection for the device operation (bulk- or injection-limitation) is simply unpractical. Therefore, the investigation of dynamic or transient properties (i.e. impedance response) could be determinant by revealing exclusive spectroscopic patterns. In this sense the work by Nguyen and Schmeits [6] on ITO/ $\alpha$ -NPD/Al devices clearly demonstrated the space-charge limited origin of the capacitance spectra. A minimum is observed in  $C(\omega)$  (reduction of about 25%) which is related to the hole transit time  $\tau_t$  and allows to determine the hole mobility  $\mu$ . For  $\alpha$ -NPD samples with thickness 1340 nm, steady-state and modulated experimental data were then consistent with a unique device model: current was space-charge limited (including trap states) by transport of holes. The negative values reached by the low-frequency capacitance at forward voltages were attributed to the additional injection of minority carriers (electrons) through the Al cathode [6].

The aim of this work was to verify whether SCLC trends are still observable in thin (<200 nm)  $\alpha$ -NPD devices when frequency-resolved techniques such as impedance spectroscopy are used. In particular we observed that  $J \ll J_{\text{SCLC}}$  by several orders of magnitude for usual operating voltages. The low-frequency capacitance exhibits positive values in excess of the geometrical capacitance at low bias. At higher bias the response changes to an inductive behavior, clearly visible as the negative values reached by the capacitance at low frequencies. Such negative capacitance response has been reported by many authors [28,30–32]. These two trends, namely the absence of SCLC features ( $J \ll J_{\text{SCLC}}$ ) and the negative values at low frequencies in the capacitance spectra, have been interpreted as strong indication of the injection-limited mechanism underlying

the device operation. The paper is structured as follows: in Section 2 ( $J$ - $V$  characteristics and capacitance spectra) are presented. It is explained how purely bulk models have difficulty interpreting the experimental results. Consequently, a hole-injection model able to simultaneously account for both steady-state and dynamic responses is described with high degree of generality in Section 3. Finally, Section 4 is devoted to the comparison between the experimental results in Section 2 and model simulations.

## 2. Experimental results

The devices used in this study had the following structure ITO/ $\alpha$ -NPD/Ag. The ITO glass ( $30 \Omega/\square$ ) was cleaned in ultrasonic baths of ethanol, acetone, soap and Milli-Q water.  $\alpha$ -NPD was purified by gradient sublimation. A 176-nm-thick film was thermally evaporated at a rate of  $1.0 \text{ \AA/s}$  at a base pressure of around  $5 \times 10^{-7}$  mbar. Ag electrodes (100 nm) were deposited in another chamber at a rate of  $11 \text{ \AA/s}$ , at a pressure of around  $2 \times 10^{-6}$  mbar, to form device active areas of  $4 \text{ mm}^2$ . For the measurements, devices were encapsulated in nitrogen atmosphere inside quartz tubes. Impedance measurements were performed using a Solartron 1260 frequency response analyzer (FRA). A dielectric interface (SI 1296) was coupled to the FRA in order to achieve higher sensitivity in the high impedance dielectric range. Oscillating amplitude of 10 mV was added to the dc bias voltage using frequencies within the range of 1 MHz down to 0.1 Hz. Capacitance spectra were obtained from the impedance  $Z$  as  $C = \text{Re}(1/i\omega Z)$ , where  $i = \sqrt{-1}$  and  $\omega$  is the angular frequency of the ac perturbation.

The  $J$ - $V$  characteristics of a  $L=176$  nm-thick ITO/ $\alpha$ -NPD/Ag device measured at room temperature is shown in Fig. 1. It is usually found that  $J$ - $V$  characteristics in OLEDs in reverse and forward bias direction up to approximately the built-in potential  $V_{\text{bi}}$  exhibits Ohmic response. This behavior is believed to be caused by additional leakage currents (shunt resistance) flowing in parallel with useful currents responsible for the device operation.  $V_{\text{bi}}$  is influenced not only by the work function offset between the contacting materials but also by possible interface dipole layers which are formed during the device fabrication [16]. For voltages more positive than  $V_{\text{bi}} \approx 1.8$  V a current increase starts indicating the voltage-driven enhancement in charge carrier injection. By examining Fig. 1(b), which results after calculating the operating voltage as  $V = V_{\text{bias}} - V_{\text{bi}}$ , one can realize that the  $J$ - $V$  characteristics approximately follows a power-law relation ( $J \propto V^m$ ) with exponent  $m \approx 7$  at  $V > 2$  V. Interestingly, the comparison between the experimental curve and that resulting from simple SCLC models (Eq. (1)) using mobility values typical for  $\alpha$ -NPD, alert us about the extremely reduced Ohmic character of the ITO/ $\alpha$ -NPD contact. At  $V = 2$  V, SCLC models predict current levels which exceed experimental data in more than four orders of magnitude. This fact leads us to consider that injection mechanisms are responsible for the measured  $J$ - $V$  characteristics.

Capacitance response under variation of the applied bias is shown in Fig. 2. One can realize that the capacitance is constant and bias-independent at high-frequencies ( $>10^5$  Hz). This flat response of  $C_0 = 0.45$  nF corresponds to the geometrical capacitance of the device and yields a permittivity of  $\epsilon = 2.24$ , typical for amorphous organic semiconductors. For bias voltages (1 V) below the injection voltage the capacitance is almost constant within the measuring frequency range. At  $V_{\text{bias}} > V_{\text{bi}}$  the capacitance grows monotonously toward lower frequencies (2 V). This feature has been usually interpreted in terms of trapping [33]. At higher bias (3 V) the capacitance values reach a maximum at intermediate frequencies ( $\sim 10$  Hz) and develop an inductive behavior in the low-frequency limit. This last feature has been linked with the injection of minority carriers [6,34], or alternatively with the injection kinetics at the interfaces [28,29,35].

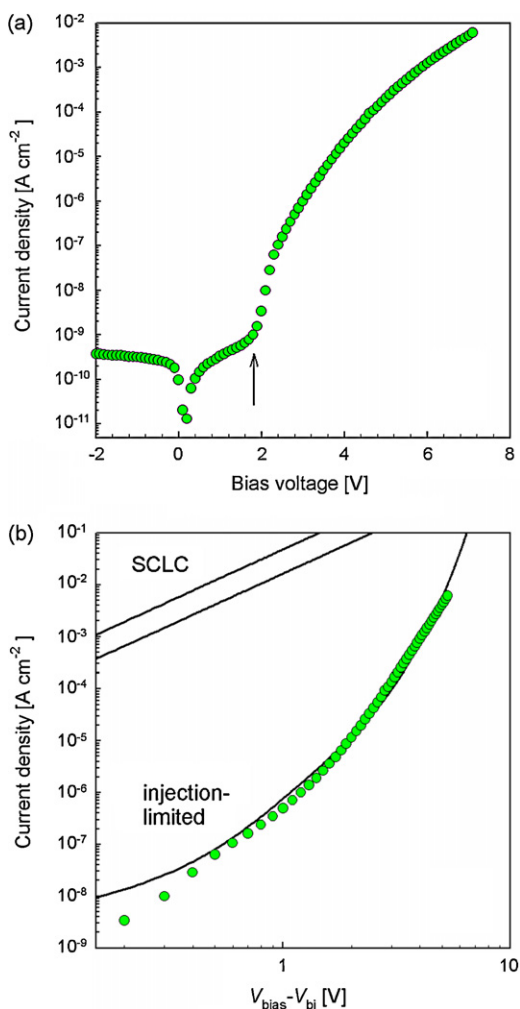


**Fig. 1.** *J*–*V* characteristics of a *L* = 176 nm-thick ITO/ $\alpha$ -NPD/Ag device measured at room temperature. (a) Complete response indicating the current injection, built-in potential (arrow). (b) Comparison between experiment (dots) and hole-injection model prediction (solid line) in a log–log representation. Model parameters:  $N_1 = 4.2 \times 10^{20} \text{ cm}^{-2}$ ,  $N_B = 10^{20} \text{ cm}^{-3}$ ,  $E_{F0} = 0.0 \text{ eV}$ ,  $E_2^* = -4 \text{ eV}$ ,  $k_B T_0 = 0.5 \text{ eV}$ ,  $E_3^* = 0 \text{ eV}$ ,  $\sigma_B = 0.1 \text{ eV}$ ,  $\alpha_1 = 1$ ,  $\alpha_2 = 0.1$ ,  $k_{12} = 1 \text{ s}^{-1}$ ,  $k_{23} N_B = 0.06 \text{ s}^{-1}$ ,  $\gamma_1 = 0.1$ , and  $\gamma_2 = 0$ . Upper solid lines correspond to SCLC derived from mobility values within the range of  $9 \times 10^{-4}$  to  $3 \times 10^{-4} \text{ cm}^2 \text{ V}^{-1} \text{ s}^{-1}$ .

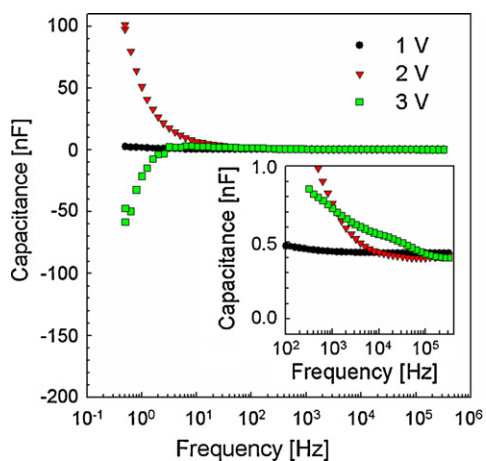


**Fig. 2.** Capacitance spectra of a *L* = 176 nm-thick ITO/ $\alpha$ -NPD/Ag device measured at room temperature measured at three different bias voltages indicated. In the inset: high-frequency detail near the geometrical capacitance value.

One might try to interpret the measured capacitance spectra in terms of SCLC ac models [6]. The hole mobility of  $\alpha$ -NPD at room temperature [4–6] is known to be within the range of 9 to  $3 \times 10^{-4} \text{ cm}^2 \text{ V}^{-1} \text{ s}^{-1}$ , what would imply transit frequencies  $> 10^6 \text{ Hz}$  for operating voltages near 1 V assuming relations like  $\mu = 4L/3\tau_t F$  [12]. Unfortunately the frequency range for the expected  $\tau_t$  lies near the upper limit of the measuring frequency as observed in the experimental capacitance spectra (inset of Fig. 2). Conversely if the measured *J*–*V* characteristics in Fig. 1 are considered to be originated by purely bulk mechanisms like SCLC, the hole mobility would lie within the range of  $10^{-8} \text{ cm}^2 \text{ V}^{-1} \text{ s}^{-1}$  and corresponding transit frequencies around 100 Hz. However, there is no feature at such frequencies signaling the occurrence of SCLC ac patterns in the inset of Fig. 2 (like the reduction of *C* towards lower frequency values).

The more distinctive feature of the capacitance spectra in Fig. 2 is the transition between positive to negative capacitance between  $V_{\text{bias}} = 1\text{--}2 \text{ V}$ . For double-carrier injection devices, negative capacitance has been understood as originated from transport of minority carriers [34,36] or related to the electron-hole recombination [37]. In the structures analyzed in this study the injection of electrons is strongly blocked by effect of the large energy offset between Ag cathode work function ( $\sim 4.5 \text{ eV}$ ) and the lowest unoccupied molecular orbital (LUMO) level of  $\alpha$ -NPD ( $\sim 2.4 \text{ eV}$ ). We can then discard recombination after electron injection as the origin for the negative capacitance observed.

### 3. Hole-injection model

Following our recent derivation of kinetic models for electron-injection at metal–organic interfaces [29], we describe here the model for hole-injection as sketched in Fig. 3. The injection from the ITO Fermi level to the organic conductor highest occupied molecular orbital (HOMO)  $E_3$  occurs sequentially, via interface states with energy  $E_2$ . We considered energetically distributed interface states and demonstrated [28] that the low-frequency (equilibrium) capacitance is proportional to the variation of the interfacial state occupancy with the bias voltage  $C_c = qN_i \Delta\theta/\Delta V$  ( $q$  denotes the positive elementary charge, and  $\theta$  is the occupancy of the interface states). The interface states are filled at low bias voltages giving increasing positive values of the low-frequency limit of the capacitance, since the interfacial density of states (IDOS) increases in the direction of variation of the Fermi level at increasing bias voltage. At some point an increment in the applied bias promotes the depopulation ( $\Delta\theta < 0$ ) of the IDOS by a net flux of holes injected into the HOMO of the bulk organic layer. The low-frequency limit of the capacitance then changes sign and becomes negative. Following this view the negative capacitance is originated by an exclusively interfacial mechanism. In the following, we present the derivation of the model using a distribution of states both in the dipole layer and in bulk levels of the organic material.

The operating positive potential  $V = V_{\text{bias}} - V_{\text{bi}}$  is:

$$V = -\frac{E_{F1} - E_{F0}}{q} \quad (2)$$

which moves the ITO Fermi level from the equilibrium  $E_{F0}$  down to a more negative position  $E_{F1}$ . One can define the potential at the cathode:

$$V_c = -\frac{E_{F1} - E_{F3}}{q} \quad (3)$$

and the potential in the bulk:

$$V_b = -\frac{E_{F3} - E_{F0}}{q} \quad (4)$$

so that  $V = V_c + V_b$ .

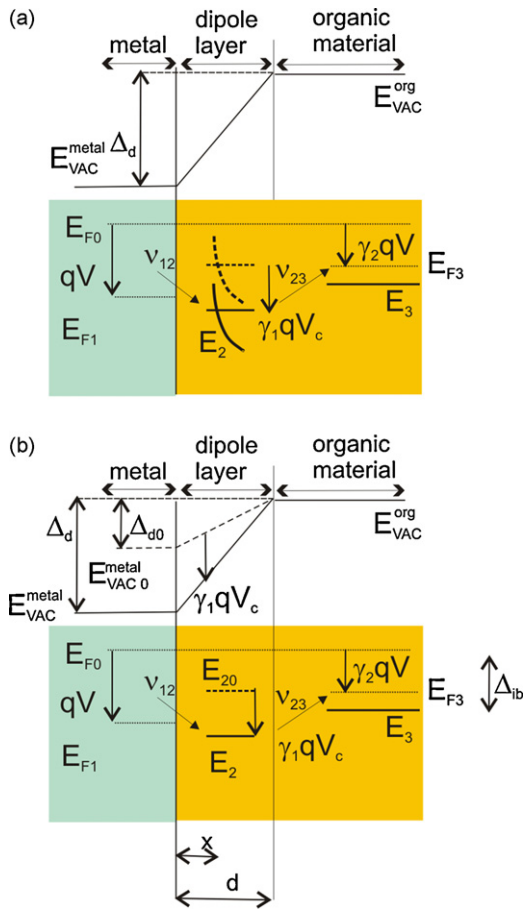


**Fig. 3.** Scheme of the injection model for a generic metal–organic interface, showing the changes under applied positive potential  $qV$ .  $E_{F0}$  is the equilibrium Fermi level and  $E_{F1}$  the Fermi level.  $E_{F3}$  corresponds to the Fermi level in the bulk of the organic material.  $E_2$  accounts for an interfacial level, and  $E_3$  for level of the bulk LUMO in the organic conductor.  $\gamma_1 qV_c$  and  $\gamma_2 qV$  represent the corresponding shift under potential application.  $v_{12}$  is the rate of transfer from metal to interfacial level, and  $v_{23}$  the rate of transfer from interfacial to bulk levels.  $\Delta_d$  represents the vacuum level discontinuity at the interface caused by the dipole layer, and  $\Delta_{ib}$  is the injection barrier. (a) Shift of the interfacial distribution. (b) Modification of the vacuum level discontinuity.

The occupation of the bulk levels at energy  $E_3$  follows the Boltzmann function as:

$$f(E_3, E_{F3}) = \exp \left[ \frac{E_3 - E_{F3}}{k_B T} \right] \quad (5)$$

Here  $E_{F3}$  accounts for the bulk organic hole Fermi level, and  $k_B T$  denotes the thermal energy. Therefore, the potential  $V_b$  determines the carrier density in the transport levels in proximity of the dipole layer. The change of occupation will have an effect on the injection model only at high carrier density, since it induces a return of injected charge from the bulk levels to the interfacial levels. For simplicity, we assume that the increase of carrier density in the bulk is determined by the parameter  $\gamma_2$ , according to the relationship:

$$E_{F3} = E_{F0} + \gamma_2(E_{F1} - E_{F0}) \quad (6)$$

Therefore, we obtain  $V_c = (1 - \gamma_2)V$ , and  $V_b = \gamma_2 V$ .

In general, the increase of charge density in bulk levels will depend on the rapidity of evacuation of the carriers, i.e. the transport model, and also on the presence of opposite sign charge carriers. Therefore, this effect will be more significant in two-carrier devices, while in single carrier devices the density remains low and we can assume  $\gamma_2 \approx 0$ .

More significant for the injection model are the modifications under an operating potential occurring at the dipole layer, of width

$d$ , where the interface levels are located. In general, intermediate states are associated with the presence of interfacial dipoles. The gap states provide the charge required to establish thermodynamic equilibrium between the metal and the organic material, and it can be considered that the interfacial levels lie within the dipole layer [38,39]. In Fig. 3(b), we assume that the interfacial levels lie a distance  $x \leq d$  from the metal surface. In equilibrium, the net effect caused by the change of dipole energy at the interface is  $\Delta_d^0$  (the vacuum level discontinuity). A positive operating voltage  $V_c$  increases  $\Delta_d = \Delta_d^0 + qV_c$  and reduces the injection barrier  $\Delta_{ib} = -(E_3 - E_{F1})$ , as shown in Fig. 3(b). The variation of  $\Delta_d$  induces a shift of the interfacial levels. As indicated in Fig. 3(b), the change of any energy level  $E_2$  is:

$$E_2 = E_{20} - q \frac{d-x}{d} V_c \quad (7)$$

We denote  $\gamma_1 = 1 - x/d$ . If  $\gamma_1 \approx 1$  the energy level  $E_2$  accompanies the variations of  $E_{F1}$ , and on the other hand, if  $\gamma_1 \approx 0$ , the interfacial level is pinned at the organic surface and remains stationary. From Eq. (7) we have:

$$E_2 = E_{20} - q\gamma_1(1 - \gamma_2)V \quad (8)$$

As we will next explain simulations match with capacitance and steady-state characteristics by assuming an exponential distribution for the IDOS [29]. The density at the interfacial energy level  $E_2$  is:

$$g_1(E_2^r - E_2) = \frac{N_1}{k_B T_0} \exp \left[ \frac{E_2^r - E_2}{k_B T_0} \right] \quad (9)$$

with respect to the reference level  $E_2^r$ . Here  $N_1$  corresponds to the total interface state density, and  $k_B T_0$  is the characteristic energy of the exponential tail. This distribution, shifts with the potential as indicated in Eq. (8) and depicted in Fig. 3(a). For the energy levels of the bulk organic material, we adopt a Gaussian DOS around  $E_3^r$ :

$$g_B(E_3^r - E_3) = \frac{N_B}{\sqrt{2\pi}\sigma_B} \exp \left[ -\frac{(E_3^r - E_3)^2}{2\sigma_B^2} \right] \quad (10)$$

being  $N_B$  the bulk total density of states, and  $\sigma_B$  the energetic disorder parameter usually assumed as a consequence of fluctuations in polarization and dipole energies [40]. In most cases a value  $\sigma_B \approx 0.1$  eV is found [41].

The rate of charge transfer *per site* between the metal and interfacial states at the energy  $E_2$  is given by the expression [28]:

$$v_{12}(E_2) = k_{12} \{ (1 - \theta)A - \theta B \} \quad (11)$$

where  $\theta$  represents the occupancy of the interface state,  $k_{12}$  the rate constant for transfer from ITO to interfacial level and:

$$A = \exp \left[ \frac{(\alpha_1 - 1)(E_{F1} - E_2)}{k_B T} \right] \quad (12)$$

$$B = \exp \left[ \frac{\alpha_1(E_{F1} - E_2)}{k_B T} \right] \quad (13)$$

Similarly, the rate of charge transfer *per site* between the interface level and the bulk organic material is:

$$v_{23}(E_2, E_3) = k_{23} \{ \theta C - f(1 - \theta)D \} \quad (14)$$

where  $k_{23}$  stands for the rate constant for transfer from interfacial to bulk levels, and:

$$C = \exp \left[ \frac{\alpha_2(E_3 - E_2)}{k_B T} \right] \quad (15)$$

$$D = \exp \left[ \frac{(\alpha_2 - 1)(E_3 - E_2)}{k_B T} \right] \quad (16)$$

In these expressions  $\alpha_1$  and  $\alpha_2$  denote the asymmetry factors of the corresponding charge transfer processes.

The expression for the current density is obtained by integration of  $v_{12}$  over the IDOS:

$$J(V) = q \int_{-\infty}^{+\infty} g_1(E_2, E_{20}) v_{12}(E_2) dE_2 \quad (17)$$

The rate of charge transfer from a  $E_2$  level to bulk organic levels is:

$$v_{23}(E_2) = k_{23} \int_{-\infty}^{+\infty} g_B(E_3, E_{30}) \{ \theta C - f(1 - \theta) D \} dE_3 \quad (18)$$

Therefore, we can write:

$$v_{23}(E_2) = k_{23} \{ \theta F - (1 - \theta) G \} \quad (19)$$

where

$$F = \int_{-\infty}^{+\infty} g_B(E_3, E_{30}) C dE_3 \quad (20)$$

$$G = \int_{-\infty}^{+\infty} g_B(E_3, E_{30}) f D dE_3 \quad (21)$$

The change of the occupancy of the intermediate levels at the energy  $E_2$  is given by:

$$\frac{d\theta(E_2)}{dt} = v_{12}(E_2) - v_{23}(E_2) \quad (22)$$

At steady state, we can solve:

$$v_{12}(E_2) - v_{23}(E_2) = 0 \quad (23)$$

and one readily obtains the occupancy of the level  $E_2$ :

$$\theta(E_2) = \frac{1}{1 + ((B + bF)/(A + bG))} \quad (24)$$

where  $b = k_{23}/k_{12}$ .

Inserting Eq. (24) in Eq. (11) we obtain the dc current from Eq. (17). Note that the term in  $G$  in Eq. (24) corresponds to the return of charge from bulk levels to interfacial levels, and can normally be neglected.

Let us denote ac modulation of quantity  $y$  by  $\Delta y$  and the Laplace variable by  $s = i\omega$ . The ac current is:

$$\Delta J = q \int_{-\infty}^{+\infty} g_1(E_2^r - E_2) \left( \frac{\partial v_{12}}{\partial \theta}(E_2) \Delta \theta + \frac{\partial v_{12}}{\partial V}(E_2) \Delta V \right) dE_2 \quad (25)$$

We obtain the admittance:

$$Y = \frac{\Delta J}{\Delta V} = q \int_{-\infty}^{+\infty} g_1(E_2^r - E_2) \left( \frac{\partial v_{12}}{\partial \theta}(E_2) \frac{\Delta \theta}{\Delta V} + \frac{\partial v_{12}}{\partial V}(E_2) \right) dE_2 \quad (26)$$

Detailed expression of the terms in parenthesis has been given in the previous work [29]. The capacitance then is defined as  $C = Y/s$ .

#### 4. Discussion

In the following we discuss on the parameters used in the simulation based on the described hole-injection model. We should emphasize that the model has to account for both steady-state and frequency-dependent characteristics with a single set of parameters giving a complete description of the charge injection process. By examining Fig. 1(b) one can realize that the  $J$ - $V$  characteristics resulting from the above outlined model [Eq. (17)] is able

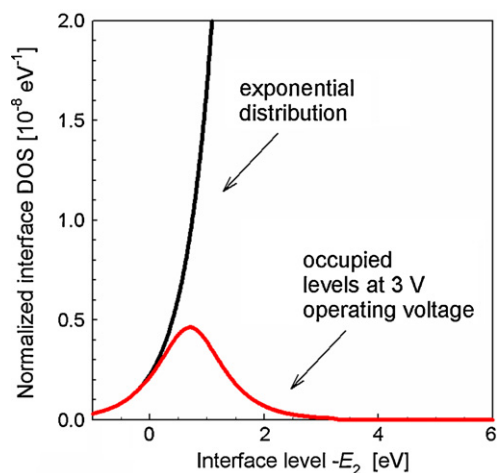


Fig. 4. Interface density-of-states IDOS following an exponential distribution and portion of such states intervening in the injection process at 3 V of operating voltage. Same set of parameters as in Fig. 1.

to reproduce with a good approximation the  $J \propto V^m$  response for bias larger than 1 V. In this simulation the total IDOS has been  $N_1 = 3.2 \times 10^{20} \text{ cm}^{-2}$ , and total bulk density of  $N_B = 10^{20} \text{ cm}^{-3}$  with  $\sigma_B = 0.1 \text{ eV}$ . The interface state shift used in the simulation corresponds to  $\gamma_1 = 0.1$ , indicating that the intermediate levels are almost pinned at the organic surface. The effective density of occupied interface states can be calculated after considering the occupancy of each state and integration of Eq. (24). For operating voltage of 3 V the effective IDOS intervening in the injection process results  $\sim 5 \times 10^{12} \text{ cm}^{-2}$ , as obtained by integration of the occupied levels in Fig. 4. It should be noted here that the order of magnitude obtained lies within typical values reported in the literature [26]. The intermediate state occupation reaches a maximum for levels located  $\sim 0.4 \text{ eV}$  below the ITO work function in equilibrium, and exhibit a Gaussian-like distribution. These levels can be then interpreted as forming an effective hole energy barrier, which is highly determined by the injection kinetics. The IDOS shown in Fig. 4 exhibit features different from those proposed to account for steady-state,  $J$ - $V$  characteristics [26]. In such analysis the interface Gaussian DOS is located within the organic band gap, and undergoes the influence of the interfacial dipoles which induce a broadening of 3–4 times the values encountered for bulk Gaussian DOS ( $\sigma_B \approx 0.1 \text{ eV}$ ). In our analysis the IDOS characteristic energy  $k_B T_0 = 0.5 \text{ eV}$  used in the simulation appears also larger than the value deduced from purely bulk SCLC models ( $\sim 0.1 \text{ eV}$ ). However, in Ref. [26] the interface states are postulated to be in equilibrium with the metal contact, in opposition to our assumptions. Moreover, one can observe in Fig. 4 that the IDOS spreads below the HOMO of the organic bulk forming an effective barrier. The energy difference between the anode Fermi level and the HOMO levels used in the simulation was  $E_3^r - E_{F0} \approx 0 \text{ eV}$ , which informs on the interfacial dipole effect on improving hole injection [21].

It is worth noting that the IDOS proposed here differs from that resulting from theoretical studies of 'ideal', weakly interacting metal–organic junctions [42]. In such non-reactive interfaces induced DOS appears by effect of the metallic contact, which forces the charge neutrality level to align the metal Fermi level [43]. We consider that the interfaces analyzed here do not belong to such category. It has been recognized that metal–organic interfaces form structurally and chemically complex structures. Diffusion and chemical reaction can lead to the formation of new complexes with a different electronic structure than that observed in the bulk of the organic film [20]. We are then inclined to believe that the IDOS resulting from our analysis reflects the characteristics of 'real'

interfaces in which chemical reaction or metal diffusion play a determining role.

The asymmetry factors (transfer coefficients) [44] for electron transfer were chosen as  $\alpha_1 = 1$  and  $\alpha_2 = 0.1$ . In case of  $E_{F1} < E_2$  the first asymmetry factor reproduces transitions of the Miller–Abrahams type [45]. When  $E_{F1} > E_2$  the back transition from intermediate states down to the metal is energetically favoured due to the positive overpotential as derived from Eqs. (12) and (13). Since  $\alpha_2 \approx 0$  the second transitions ( $2 \leftrightarrow 3$ ) are also governed by a mechanism similar to that encountered for  $1 \leftrightarrow 2$ , as one can see from Eqs. (15) and (16). It should be noted here that strict Miller–Abrahams-type transitions derive from hydrogen-like wave functions with spherical symmetry. It is then not surprising that hopping transition at the interface deviate from this simple form.

Influence of the hopping rates is observed in the simulated capacitance spectra of Fig. 5, which result from the capacitance derived from Eq. (26) plus the geometrical capacitance. A net rate constant  $k'_{23}$  for the second transitions from interfacial to bulk levels can be defined by integration of Eqs. (20) and (21). The total DOS of the bulk HOMO modifies the net rate as  $k'_{23} = k_{23}N_B$ . Since  $k_{12} > k'_{23}$  ( $k_{12} = 1 \text{ s}^{-1}$ ,  $k'_{23} = 0.06 \text{ s}^{-1}$ ) the effect of the interface state depopulation appears at lower frequencies, which allows the increment in the capacitance at intermediate frequencies (curves corresponding to  $V \geq 1 \text{ V}$  in Fig. 5) related to the transient filling of interface states. Note here that the simulation captures the essential features of the experimental curves in Fig. 2. For both experimental (Fig. 2) and simulated spectra (Fig. 5), low-frequency capacitance exhibits a transition between positive to negative values within a voltage change as low as 1V. There are, however, differences between experimental and simulation curves that we tentatively attribute to possible dependences of the transition rate constants on the operating voltage.

Positive values of the excess capacitance have been previously proposed to derive from filling of bulk trap states [6,31]. Therefore, bulk models point to two different types of charge carriers to interpret the capacitance measurements. Whereas  $\Delta C = C - C_0 < 0$  occurs as a consequence of reducing the amount of minority free carriers (electrons),  $\Delta C > 0$  is believed to be related to the occupancy of traps. On the contrary, our approach simplifies the picture by seeing the evolution in the occupancy of interface states as responsible for the whole capacitance spectra change with operating voltage. It must be stressed that some aspects remain unclear and need further work. Particularly, the observed slow kinetics of the filling/releasing process of interface states governing the carrier injection. This observation suggests us that not only the interface

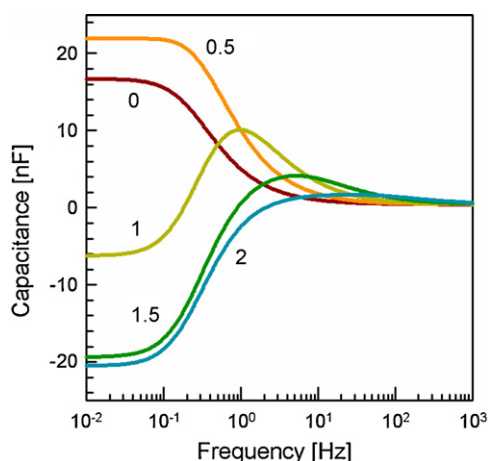


Fig. 5. Simulated capacitance spectra using the same set of parameters as in Fig. 1 for different values of the operating voltage as indicated (in V).

energetics plays a determining role in the injection process but also the kinetics of occupancy may have great influence for device operation.

## 5. Conclusions

We have obtained a coherent picture about the injection processes governing thin (<200 nm) ITO/ $\alpha$ -NPD/Ag hole-only devices. A detailed model for the impedance of the carrier injection is provided that highlights the role of the filling/releasing kinetics of energetically distributed interface states. The injection-model proposed is able to account for both steady-state ( $J$ - $V$  characteristics), and alternating current response (capacitance spectra). Values exhibited by the capacitance at low frequencies are in agreement with the kinetic of occupation of interface states. The effective density of occupied interface states results  $\sim 5 \times 10^{12} \text{ cm}^{-2}$ . The intermediate state occupation reaches a maximum for levels located  $\sim 0.4 \text{ eV}$  below the ITO work function in equilibrium, and exhibits a Gaussian-like distribution. These levels can be then interpreted as forming an effective hole energy barrier, which is highly determined by the injection kinetics. As a final conclusion we can say that deeper knowledge of the physico-chemical characteristics of such interface states and their relation to and influence of the dipole layer appears to be crucial for tailoring properties of thin-film organic devices.

## Acknowledgments

We thank financial support from Ministerio de Educacion y Ciencia under project HOPE CSD2007-00007 (Consolider-Ingenio 2010). We acknowledge F. Nüesch and L. Zuppirolli for help in sample preparation.

## References

- [1] J. Shinar, Organic Light-Emitting Devices. A Survey, Springer-Verlag, New York, 2004.
- [2] K. Müllen, U. Scherf, Organic Light-Emitting Diodes. Synthesis, Properties, and Applications, Wiley-VCH, Weinheim, 2006.
- [3] S.A. van Slyke, C.H. Chen, C.W. Tang, Applied Physics Letters 69 (1996) 2160.
- [4] Z. Deng, S.T. Lee, D.P. Webb, Y.C. Chan, W.A. Gambling, Synthetic Metals 107 (1999) 107.
- [5] E.W. Forsythe, M.A. Abkowitz, Y. Gao, C.W. Tang, Journal Vacuum Science Technology A 18 (2000) 1869.
- [6] N.D. Nguyen, M. Schmeits, H.P. Loeb, Physical Review B 75 (2007) 075307.
- [7] P.E. Burrows, Z. Shen, V. Bulovic, D.M. McCarty, S.R. Forrest, J.A. Cronin, M.E. Thompson, Journal of Applied Physics 79 (1996) 7991.
- [8] M. Stössel, J. Staudigel, F. Steuber, J. Blässing, J. Simmerer, Applied Physics Letters 76 (2000) 115.
- [9] S. Berleb, A.G. Mückl, W. Brütting, M. Schwoerer, Synthetic Metals 111–112 (2000) 341.
- [10] W. Brütting, S. Berleb, A.G. Mückl, Synthetic Metals 122 (2001) 99.
- [11] C. Tanase, E.J. Meijer, P.W.M. Blom, D.M. de Leeuw, Physical Review Letters 91 (2003) 216601.
- [12] M.A. Lampert, P. Mark, Current Injection in Solids, Academic Press, New York, 1970.
- [13] Y. Shen, A.R. Hosseini, M.H. Wong, G.G. Malliaras, Chemical Physics Physical Chemistry 5 (2004) 16.
- [14] I.G. Hill, A. Kahn, Journal of Applied Physics 86 (1999) 2116.
- [15] N. Koch, A. Kahn, J. Ghijsen, J.J. Pireaux, J. Schwartz, R.L. Johnson, A. Elschner, Applied Physics Letters 82 (2003) 70.
- [16] W.R. Salaneck, K. Seki, A. Kahn, J.-J. Pireaux, Conjugated Polymer and Molecular Interfaces. Science and Technology for Photonic and Optoelectronic Applications, Marcel Dekker, New York, 2002.
- [17] A. Kahn, N. Koch, W. Gao, Journal of Polymer Science Part B: Polymer Physics 41 (2003) 2529.
- [18] X. Crispin, V. GEskin, A. Crispin, J. Cornil, R. Lazzaroni, W.R. Salaneck, J.-L. Bredas, Journal of American Chemical Society 124 (2002) 8131.
- [19] H. Peisert, M. Knupfer, T. Schwieger, J.M. Auerhammer, M.S. Golden, J. Fink, Journal of Applied Physics 91 (2002) 4872.
- [20] C. Shen, A. Kahn, I. Hill, in: W.R. Salaneck, K. Seki, A. Kahn, J.-J. Pireaux (Eds.), Conjugated Polymer and Molecular Interfaces, Marcel Dekker, Inc., New York, 2002.
- [21] D.J. Milliron, I.G. Hill, C. Shen, A. Kahn, J. Schwartz, Journal of Applied Physics 87 (2000) 572.

- [22] A. Wan, J. Hwang, F. Amy, A. Kahn, *Organic Electronics* 6 (2005) 47.
- [23] P.R. Emtage, J.J. O'Dwyer, *Physical Review Letters* 16 (1966) 356.
- [24] V.I. Arkhipov, E.V. Emelianova, Y.H. Tak, H. Bässler, *Journal of Applied Physics* 84 (1998) 848.
- [25] U. Wolf, V.I. Arkhipov, H. Bässler, *Physical Review B* 59 (1999) 7507.
- [26] M.A. Baldo, S.R. Forrest, *Physical Review B* 64 (2001) 085201.
- [27] B.N. Limketkai, M.A. Baldo, *Physical Review B* 71 (2005) 085207.
- [28] J. Bisquert, G. Garcia-Belmonte, A. Pitarch, H.J. Bolink, *Chemical Physics Letters* 422 (2006) 184.
- [29] G. Garcia-Belmonte, J. Bisquert, P.R. Bueno, C.F.O. Graeff, *Chemical Physics Letters* 455 (2008) 242.
- [30] I.N. Hulea, R.F.J. van der Scheer, H.B. Brom, B.M.W. Langeveld-Voss, A. van Dijken, K. Brunner, *Applied Physics Letters* 83 (2003) 1246.
- [31] H.H.P. Gommans, M. Kemerink, G.G. Andersson, R.M.T. Pijper, *Physical Review B* 69 (2004) 155216.
- [32] F.A. Castro, P.R. Bueno, C.F.O. Graeff, F. Nüesch, L. Zuppiroli, L.F. Santos, R.M. Faria, *Applied Physics Letters* 87 (2005) 013505.
- [33] H.C.F. Martens, H.B. Brom, P.W.M. Blom, *Physical Review B* 60 (1999) R8489.
- [34] H.H.P. Gommans, M. Kemerink, R.A.J. Janssen, *Physical Review B* 72 (2005) 235204.
- [35] G. Garcia-Belmonte, H.J. Bolink, J. Bisquert, *Physical Review B* 75 (2007) 085316.
- [36] M. Schmeits, *Journal of Applied Physics* 101 (2007) 084508.
- [37] E. Ehrenfreund, C. Lungenschmied, G. Dennier, H. Neugebauer, N.S. Saricifti, *Applied Physics Letters* 91 (2007) 012112.
- [38] C. Shen, A. Kahn, *Organic Electronics* 2 (2001) 89.
- [39] J.X. Tang, C.S. Lee, T.S. Lee, Y.B. Xu, *Chemical Physics Letters* 396 (2004) 92.
- [40] R.H. Young, *Philosophical Magazine B* 72 (1995) 435.
- [41] J. Bisquert, G. Garcia-Belmonte, J. García-Cañadas, *Journal of Chemical Physics* 120 (2004) 6726.
- [42] H. Vázquez, F. Flores, R. Oszwaldowski, J. Ortega, R. Pérez, A. Kahn, *Applied Surface Science* 234 (2004) 107.
- [43] H. Vázquez, Y.J. Dappe, J. Ortega, F. Flores, *Applied Surface Science* 254 (2007) 378.
- [44] A.J. Bard, L.R. Faulkner, *Electrochemical Methods. Fundamentals and Applications*, John Wiley & Sons, New York, 1980.
- [45] Y.N. Gartstein, E.M. Conwell, *Chemical Physics Letters* 217 (1994) 41.